OPEN ACCESS
IOP Publishing

Letters
Reports on Progress in Physics

Rep. Prog. Phys. **87** (2024) 080502 (7pp)
https://doi.org/10.1088/1361-6633/ad6585

Letter

Observation of a phase transition from a continuous to a discrete time crystal

Phatthamon Kongkhambut[1,6], Jayson G Cosme[2,6], Jim Skulte[1,3], Michelle A Moreno Armijos[4], Ludwig Mathey[1,3], Andreas Hemmerich[1,3,*] and Hans Keßler[1,5,*]

[1] Zentrum für Optische Quantentechnologien and Institut für Quantenphysik, Universität Hamburg, 22761 Hamburg, Germany
[2] National Institute of Physics, University of the Philippines, Diliman, Quezon City 1101, Philippines
[3] The Hamburg Center for Ultrafast Imaging, 22761 Hamburg, Germany,
[4] Instituto de Física de São Carlos, Universidade de São Paulo, São Carlos, SP 13560-970, Brazil
[5] Physikalisches Institut, Rheinische Friedrich-Wilhelms-Universität, 53115 Bonn, Germany

E-mail: hemmerich@physnet.uni-hamburg.de and hkessler@physnet.uni-hamburg.de

Received 1 February 2024, revised 8 July 2024
Accepted for publication 16 July 2024
Published 26 July 2024

Corresponding editor: Dr Lorna Brigham

Abstract

Discrete (DTCs) and continuous time crystals (CTCs) are novel dynamical many-body states, that are characterized by robust self-sustained oscillations, emerging via spontaneous breaking of discrete or continuous time translation symmetry. DTCs are periodically driven systems that oscillate with a subharmonic of the external drive, while CTCs are continuously driven and oscillate with a frequency intrinsic to the system. Here, we explore a phase transition from a continuous time crystal to a discrete time crystal. A CTC with a characteristic oscillation frequency ω_{CTC} is prepared in a continuously pumped atom-cavity system. Modulating the pump intensity of the CTC with a frequency ω_{dr} close to $2\omega_{\mathrm{CTC}}$ leads to robust locking of ω_{CTC} to $\omega_{\mathrm{dr}}/2$, and hence a DTC arises. This phase transition in a quantum many-body system is related to subharmonic injection locking of non-linear mechanical and electronic oscillators or lasers.

Supplementary material for this article is available online

Keywords: time crystal, quantum gases, Bose–Einstein condensate, phase transition, spontaneous symmtry breaking

1. Introduction

The conceptual idea of time crystals (TCs) was first described as a self-sustaining oscillatory behavior in biological systems [1], and then established as a dynamical many-body state in physical systems in [2, 3]. A defining feature of these states is the spontaneous breaking of discrete or continuous time translation symmetry, giving rise to robust oscillatory motion in an extended region of their parameter space. Two distinct scenarios for the emergence of these states are as follows: Firstly, for closed systems, the continuous time translation symmetry (CTTS) can be explicitly broken by a periodic external drive and the remaining discrete time translation symmetry (DTTS) is spontaneously broken by an oscillatory response of the system with a period longer than that of the

[6] These two authors contributed equally.
[*] Authors to whom any correspondence should be addressed.

drive. An ergodicity slowdown mechanism prevents the system from heating up to an infinite temperature for long times [4, 5]. This scenario is referred to as a 'discrete TC' (DTC). Secondly, a TC state can also arise for open systems coupled to a bath. Similar to the DTC in closed systems, a periodic drive triggers a subharmonic oscillatory motion of the system, resulting in a dissipative DTC. The appropriately designed bath can act as a sink for the entropy produced by the system. [6]. We note that, in contrast to closed systems, in open systems, a TC can also emerge in the absence of periodic driving, resulting in the spontaneous breaking of CTTS. This dynamical state is referred to as a 'continuous TC' (CTC) [7–9].

The theoretical conceptualization of TCs in the context of many-body physics was followed by rapid experimental progress. DTCs in nearly closed systems have been realized in arrays of trapped ions, nitrogen vacancy centers, and in a mechanically kicked Bose–Einstein condensate (BEC) [10–12]. Discrete dissipative TCs were demonstrated in a BEC of neutral atoms in an optical cavity [13–16] and in an optical microcavity filled with a Kerr medium [17]. Finally, continuous dissipative TCs were, for example, realized in magnon BECs [18], BECs of neutral atoms [19], in collections of spins in a semi-conductor matrix [20], in photonic metamaterials [21], or doped crystals [22].

Injection locking (IL) is a phenomenon, which can arise if a nonlinear dissipative oscillator in a limit-cycle state [23], that is driven externally with a driving frequency $\omega_{\rm dr}$. For sufficiently strong driving, the oscillator locks to the external drive. This locking can occur at the driving frequency itself, or, more generally, at a rational ratio of the driving frequency [24, 25]. A specific case is subharmonic IL, in which the phase-locking occurs at an integer fraction of the driving frequency, i.e. $\omega_{\rm dr}/n$ with $n \in \{1, 2, \ldots\}$. We note that IL is a key phenomenon in electronic circuits, laser systems, and biological systems, such as the circadian rhythms of organisms [26] or the synchronization of flashing of fireflies exposed to a periodically switching torch [27]. In biological systems or mathematical science this phenomenon is referred to as entrainment [23].

2. Results

In this article, we demonstrate subharmonic IL in the context of time crystals. Here, a limit cycle is provided by a CTC produced in an atom-cavity system, oscillating at a frequency $\omega_{\rm CTC}$. We drive the system with a perturbation with a frequency $\omega_{\rm dr}$, which is close to $2\,\omega_{\rm CTC}$. As a result, the CTC locks to the driving frequency, performing an oscillatory motion at $\omega_{\rm dr}/2$, i.e. at a subharmonic frequency. In the language of time crystals, we realize a non-equilibrium phase transition between a CTC and DTC. In the terminology of laser physics, we establish subharmonic IL in a quantum many-body system.

Our setup is shown in figure 1(a). We start with a CTC prepared in an atom-cavity system (cf figure 1(a)) consisting of a BEC located in a high-finesse optical cavity, pumped transversally by an optical standing wave at constant intensity. As reported in [19], this leads to robust self-sustained oscillations of the intra-cavity photon number $N_{\rm P}(t)$, which establishes a CTC. Its frequency $\omega_{\rm CTC}$ can be associated with the emergence of a limit cycle [8, 28–32]. As seen in figure 1(b), the oscillation of the CTC breaks the CTTS. The real and imaginary parts of the Fourier spectrum of $N_{\rm P}(t)$ at the dominant frequency $\omega_{\rm CTC}$ are plotted here for different experimental implementations. The phase values of the Fourier spectra are randomly distributed between 0 and 2π, confirming the expected spontaneous breaking of CTTS.

Next, we modulate the intensity of the pump field $\varepsilon(t)$ at a frequency $\omega_{\rm dr}$ close to $2\omega_{\rm CTC}$. The periodic drive breaks the CTTS of the atom-cavity platform such that the modulated system only retains DTTS. Under the influence of the modulation, the system converts into a DTC (see [14]) with an oscillation frequency $\omega_{\rm DTC}$ approaching $\omega_{\rm dr}/2$ for sufficiently strong driving. In figure 1(c), we analyze the Fourier spectra at the emission frequency $\omega_{\rm DTC}$ for different experimental implementations. Only two almost equiprobable (49% and 51%) phase values, approximately differing by π, are observed, confirming spontaneous breaking of the DTTS (cf video in the supplementary information [33]). The modulation, in addition to the observed frequency pulling towards subharmonic response, also gives rise to a line narrowing of the DTC emission as presented in the histogram in figure 1(d). This is also seen in figures 1(e) and (f), showing that the oscillations observed in $N_{\rm P}(t)$ become more regular as the modulation sets in at $t = 0$ and the lifetime of the TC extends to more than a hundred driving cycles. The life time in both regimes, CTC and DTC, is mainly limited by atom loss from the trap and the associated decrease of the collective atom-light coupling.

We note that the transition of the CTC to the DTC occurs in two steps, as f_0 is increased from zero to a value above the critical value of the DTC phase. As we demonstrate in the supplementary information (cf figure 9), the intermediate regime is a quasicrystalline state [18, 34], in which the limit cycle dynamics of the CTC state transitions to a limit torus dynamics. In the frequency representation $N_{\rm P}(\omega)$, this transitions manifests itself as side-bands close to the dominant frequency peak $\omega_{\rm CTC}$ at frequencies $\omega_{\rm CTC} \pm (\omega_{\rm CTC} - \omega_{\rm dr}/2$. When f_0 is further increased above a critical value of the DTC phase, the dominant emission is shifted towards $\omega_{\rm dr}/2)$ and all side bands disappear. Hence, a phase transition towards a DTC arises. We find this intermediate limit torus regime not to be detectable experimentally, in the regime and in the experimental setup used here, due to the finite lifetime of the atoms, and other imperfections that limit the frequency resolution.

3. Methods

The experimental set-up consists of a Bose–Einstein condensate (BEC) of $N_{\rm a} = 4 \times 10^4$ ^{87}Rb atoms strongly coupled to a single mode of an optical high-finesse cavity. The system is pumped transversally, perpendicular to the cavity axis at a wavelength of $\lambda_{\rm p} = 791.59\,$nm (cf figure 1(a)). The pump light is blue detuned with respect to the relevant atomic transition, the D_1-line of ^{87}Rb at 794.98 nm. The effective pump-cavity detuning is chosen to be negative for all experiments presented

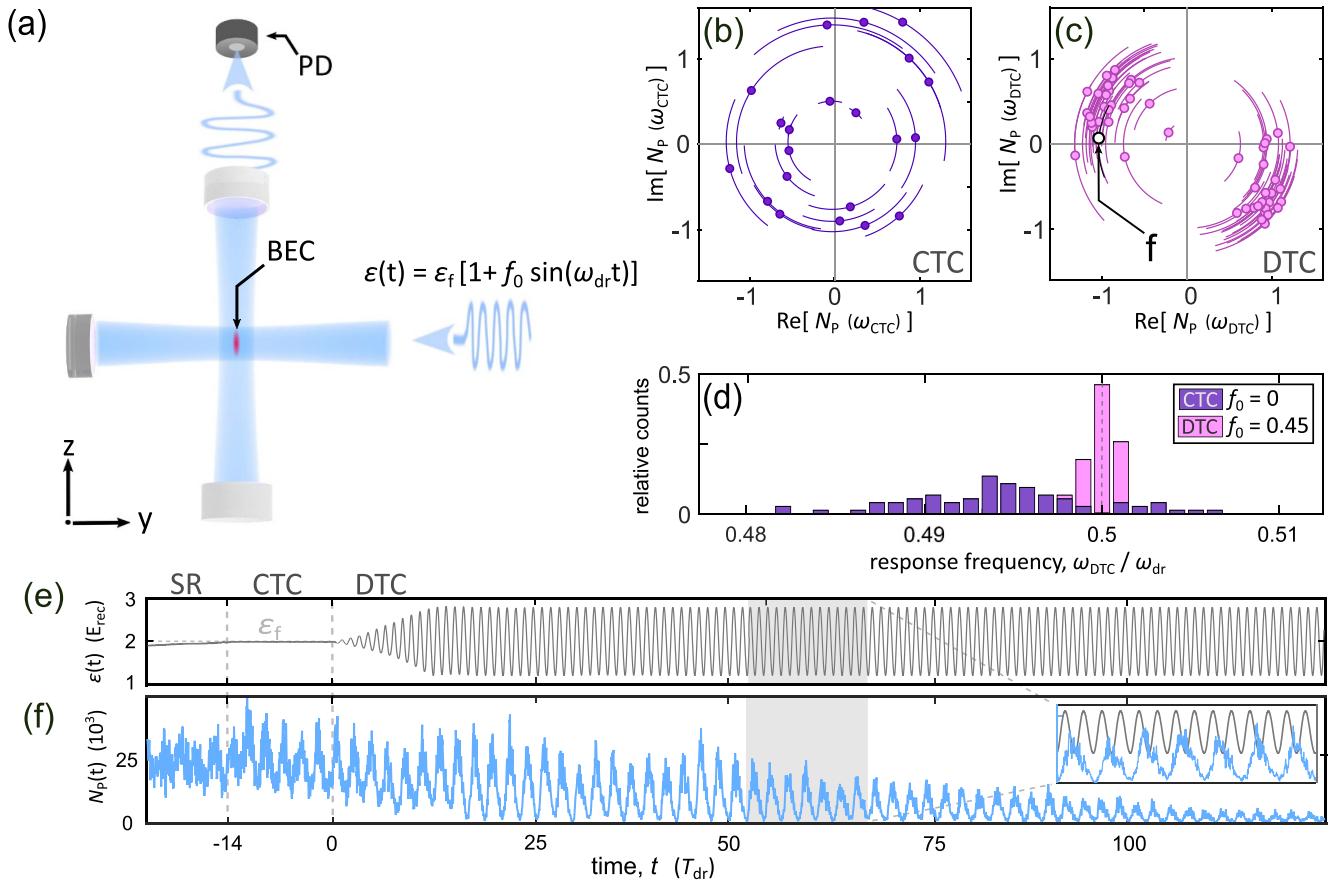

Figure 1. (a) Schematic sketch of the atom-cavity system psystem, which is periodically pumped by an optical standing wave potential transverse to the cavity axis. (b) and (c) Distributions of the time phase intra-cavity photon number $N_{\mathrm{P}}(t)$ oscillating with the main response frequencies ω_{CTC} in the CTC case shown in (b) and ω_{DTC} in the DTC case shown in (c). The error bars represent the phase uncertainty within the discrete FFT resolution of 100 Hz. The uncertainty with regard to the radial dimension, i.e. the amplitude uncertainty, is negligibly small. Note that the tilt of the two observed phase values by an angle of about $\pi/4$ with respect to the modulation signal is due to the retardation of the cavity field dynamics, which is caused by the small cavity bandwidth.. (d) Histogram of the relative number of counts of the response frequency ω_{DTC} in units of the driving frequency $\omega_{\mathrm{dr}} = 2\pi \times 22.5\,\mathrm{kHz}$ for the non-modulated ($f_0 = 0$) case in purple (dark) and the modulated case ($f_0 = 0.45$) in pink (bright), respectively. Here, the same data is used as for (b) and (c), respectively. (e) Pump protocol and (f) evolution of $N_{\mathrm{P}}(t)$ for a typical experimental realization. Below $t = -14\,T_{\mathrm{dr}}$ (first dashed vertical line), $\varepsilon(t)$ is ramped up while the systems is in the superradiant (SR) phase, indicated by a non-zero, non-oscillatory $N_{\mathrm{P}}(t)$. Between $t = -14\,T_{\mathrm{dr}}$ and $t = 0\,T_{\mathrm{dr}}$, $\varepsilon(t)$ reaches a critical value ε_{f} and the CTC phase arises, displayed by an oscillatory $N_{\mathrm{P}}(t)$. Above $t = 0\,T_{\mathrm{dr}}$ (second dashed vertical line), modulation results in a DTC, indicated by an oscillatory $N_{\mathrm{P}}(t)$ with a significantly lower bandwidth than that of the CTC (cf (d). The inset in (f) shows a zoom of $\varepsilon(t)$ and $N_{\mathrm{P}}(t)$ for the time interval marked by the gray rectangle. The effective cavity pump detuning is $\delta_{\mathrm{eff}} = -2\pi \times 8.2$ kHz and the final pump strength $\varepsilon_{\mathrm{f}} = 2.0\,E_{\mathrm{rec}}$ for all measurements presented in the main text.

here and is defined as $\delta_{\mathrm{eff}} \equiv \delta_c - \delta_-$, where $\delta_c \equiv \omega_{\mathrm{p}} - \omega_{\mathrm{c}}$ is the detuning between the pump field frequency ω_{p} and the cavity resonance frequency ω_{c}, and $\delta_- = \frac{1}{2}N_{\mathrm{a}}U_0$ denotes the collective light shift of the cavity resonance caused by the atomic ensemble for the relevant left circular polarisation mode of the cavity. For the chosen pump wavelength λ_{p}, the light shift per photon is $U_0 = 2\pi \times 0.7\,\mathrm{Hz}$. The cavity operates in the recoil resolved regime, meaning that the field decay rate of the cavity $\kappa = 2\pi \times 3.2$ kHz, which sets the time scale for the intra-cavity light field dynamics, is comparable to the recoil frequency $\omega_{\mathrm{rec}} = 2\pi \times 3.7$ kHz. The latter sets the time scale for the density distribution of the BEC to adapt to changes of the intra-cavity light field [35, 36]. This unique regime is a key prerequisite for the existence of the time crystalline phases [13, 14, 19], which are the starting point of the work presented here. The experimental cycle starts with preparing a CTC. For this, we first prepare the superradiant (SR) phase [36–39] by linearly increasing the pump-field strength $\varepsilon(t)$. When ε exceeds a critical value, we observe a non-zero intra-cavity photon number N_{P}, indicating the formation of the SR phase, in which the atoms self-organize to form a density wave that enables superradiant scattering of pump light into the cavity mode. The phase transition to the SR phase goes along with spontaneous breaking of a $\mathbb{Z}_2$ translation symmetry in space [40]. Increasing $\varepsilon(t)$ further and holding it at a constant value $\varepsilon = \varepsilon_{\mathrm{f}}$, for appropriate settings of δ_{eff} and ε_{f}, causes the system to develop periodic motion, corresponding to a CTC [19]. Subsequently, the pump strength is modulated according to $\varepsilon(t) = \varepsilon_{\mathrm{f}}[1 + f_0 \cos(\omega_{\mathrm{dr}} t)]$, with the mean pump strength ε_{f}, driving strength f_0, and frequency ω_{dr}. If the driving strength f_0

is sufficiently large, the response frequency ω_{DTC} locks to the first subharmonic of ω_{dr} and a DTC is realized (cf figures 1(e) and (f)). Note that, in contrast to the DTC observed in [13], here the system does not periodically switch back and forth between the two density gratings associated with the two symmetry broken states of the SR phase but spontaneously chooses one or the other.

4. Discussion

As a first experiment, we identify the optimal parameter values of f_0 and ω_{dr} where the IL of the CTC works most efficiently. We fix the effective detuning $\delta_{\mathrm{eff}} = -2\pi \times 8.2\,\mathrm{kHz}$ and the final pump strength $\varepsilon_{\mathrm{f}} = 2.0\,E_{\mathrm{rec}}$. For these parameters, we observed the strongest subharmonic response while keeping f_0 and ω_{dr} fixed (cf figure 1 in the supplementary information [33]). The protocol used for the measurement presented in figure 2 is as follows: We linearly increase the pump strength $\varepsilon(t)$ to its desired final value $\varepsilon_{\mathrm{f}} = 2.0\,E_{\mathrm{rec}}$ for fixed $\delta_{\mathrm{eff}} = -2\pi \times 8.2\,\mathrm{kHz}$. This is followed by a waiting time and a linear ramp-up of the driving strength f_0, both with a duration of 0.5 ms. Then, we hold all the pump parameters constant, record $N_{\mathrm{P}}(t)$ during 10 ms, and calculate the Fourier transform $N_{\mathrm{P}}(\omega)$ of $N_{\mathrm{P}}(t)$ (using a Fast Fourier transform method (FFT)). To quantify the degree of IL, we extract the subharmonic response $S = N_{\mathrm{P}}(\omega_{\mathrm{dr}}/2)/\mathrm{Max}_{\{\omega_{\mathrm{dr}},f_0\}}[N_{\mathrm{P}}(\omega_{\mathrm{dr}}/2)]$, which is the amplitude of the single-sided spectrum at half of the driving frequency $N_{\mathrm{P}}(\omega_{\mathrm{dr}}/2)$, normalized to its maximal value observed across the considered portion of the $\{\omega_{\mathrm{dr}},f_0\}$-space.

In figure 2(a), we observe a large area showing a strong subharmonic response S. For the optimal choice of δ_{eff} and ε_{f} (see supplementary information [33]), S is increased more than fourfold when compared to its value without modulation. The maximal value of S arises for a driving frequency ω_{dr} close to twice the CTC frequency ω_{CTC}, where $\omega_{\mathrm{CTC}} \approx 2\pi \times 11\,\mathrm{kHz}$ for the optimal choice of δ_{eff} and ε_{f}. The optimal driving strength of about $f_0 = 0.45$ exceeds the value predicted in our simulations (cf supplementary information [33] figure 6(a)), which may be attributed to the limited experimental lifetime and the contact interaction of the BEC, which is not accounted for in the calculations. For increasing f_0, the synchronization happens faster and is more robust in the sense that larger values of the subharmonic response S are observed together with an extension over longer time periods. Based upon the observation of spontaneous breaking of DTTS (cf figure 1(d)) and robustness of the subharmonic response against temporal perturbations of all four pump and modulation parameters $(\delta_{\mathrm{eff}},\varepsilon_{\mathrm{f}},\omega_{\mathrm{dr}},f_0)$, we claim to observe a transition between a CTC and a DTC (see supplementary information for details [33]). We investigate this transition further for a fixed driving frequency $\omega_{\mathrm{dr}} = 2\pi \times 22.5\,\mathrm{kHz}$. For each experimental realization, we obtain the Fourier spectrum as described above, but instead of considering its amplitude at $\omega_{\mathrm{dr}}/2$, we fit a Gaussian to extract the dominant response frequency ω_{DTC} as the frequency at the maximum of the Gaussian and its corresponding amplitude. These quantities are plotted versus

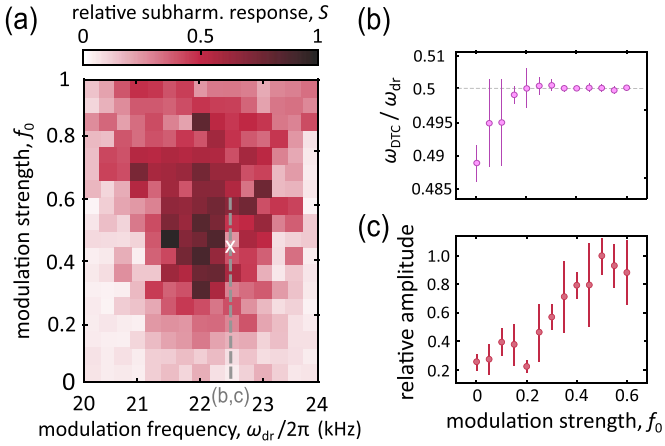

Figure 2. (a) Relative subharmonic response S versus driving strength f_0 and frequency ω_{dr} for fixed effective detuning $\delta_{\mathrm{eff}} = -2\pi \times 8.2$ kHz and final pump strength $\varepsilon_{\mathrm{f}} = 2.0\,E_{\mathrm{rec}}$. To obtain (a), we ramped the pump strength $\varepsilon(t)$ to its final value ε_{f} for fixed δ_{eff}. After a 0.5 ms long hold time, the driving strength is ramped to its desired value f_0 for a selected driving frequency ω_{dr} within 0.5 ms and subsequently held constant for 10 ms. The parameter space is divided into 15×18 plaquettes and averaged over 5 to 10 experimental realizations. The white cross indicates the parameter values $f_0 = 0.45\,\mathrm{kHz}$ and $\omega_{\mathrm{dr}} = 2\pi \times 22.5\,\mathrm{kHz}$, which are used for the measurements in figures 1(c)–(f), 3 and 4. (b) Response frequency ω_{DTC} in units of the driving frequency ω_{dr}, plotted versus the driving strength f_0. ω_{DTC} is extracted as the position of a Gaussian fit to the Fourier spectrum of the intra-cavity photon number $N_{\mathrm{P}}(t)$. (c) Relative amplitude of the main spectral component at frequency ω_{DTC}, plotted versus f_0. The plots in (b) and (c) correspond to the path marked in (a) by the gray dashed line. The error bars show the standard deviation and hence represent the shot-to-shot fluctuations.

the driving strength f_0 in figures 2(b) and (c), respectively. For increasing f_0, the response frequency ω_{DTC} approaches the value $\omega_{\mathrm{dr}}/2$. Each data point is an average of around ten experimental realizations and the error bars in figures 2(b) and (c) indicate the standard deviation, representing shot-to-shot fluctuations. These fluctuations are due to atom number variations in the BEC, originating from a combination of inherent quantum noise and technical instabilities. Interestingly, we find that for sufficiently strong driving, the emergence of the DTC is accompanied by a strong suppression of the shot-to-shot fluctuations of ω_{DTC} (cf figure 2(b)), while at the same time, the relative amplitude of the dominant spectral component at frequency ω_{DTC} increases by almost a factor of 5 (cf figure 2(c)).

To further assess the efficiency of the IL process with respect to frequency pulling and locking, we plot in figure 3 the response frequency ω_{DTC}, averaged over about ten experimental realizations, against the driving strength f_0, using three different modulation waveforms: sinusoidal (blue circles), square wave (red squares), and sawtooth (green diamonds). The protocol is otherwise the same as the one described in the previous paragraph. For all three waveforms, ω_{DTC} is pulled towards $\omega_{\mathrm{dr}}/2$ for sufficiently strong driving strength and we observe a plateauing of ω_{DTC} above $f_0 \approx 0.3$. The shot-to-shot fluctuations, given by the error bars, are seen to

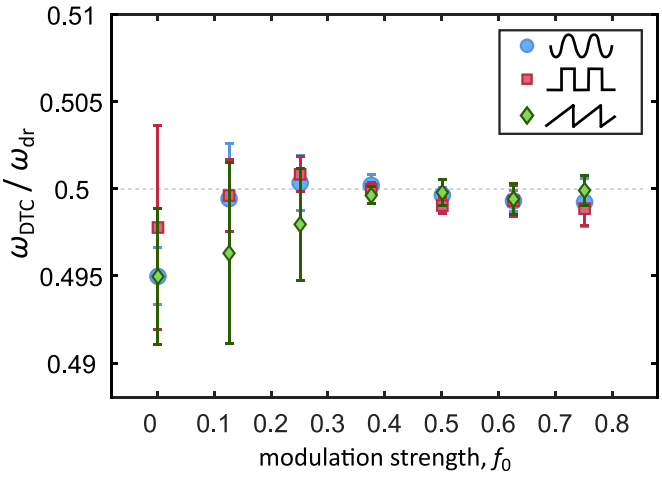

Figure 3. The blue markers show the response frequency ω_{DTC} in units of the driving frequency ω_{dr} plotted versus the driving strength f_0 for a sinusoidal modulation waveform as used for the measurements presented in figures 1, 2 and 4. The error bars show the standard deviation and hence represent the shot-to-shot fluctuations, which are strongly suppressed with increasing values of f_0. The red (square) and green (diamond) markers show the cases of modulation with square wave or sawtooth waveforms, respectively. The experimental protocol is the same as for the measurements in figures 2(b) and (c).

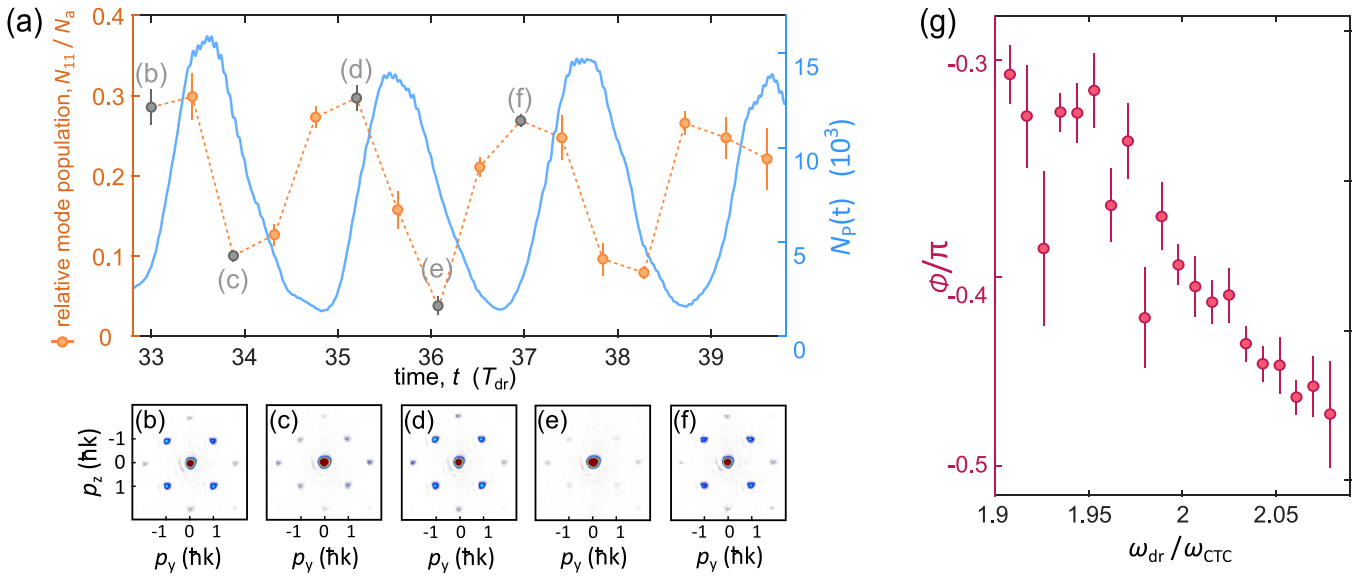

Figure 4. (a) Blue solid line: intra-cavity photon number $N_{\mathrm{P}}(t)$ averaged over five experimental realizations. Orange and gray markers: N_{11}/N_{a}, sum of the populations of the four momentum modes $\{p_{\mathrm{y}}, p_{\mathrm{z}}\} = \{\pm 1, \pm 1\}\hbar k$ normalized to the total atom number N_{a}. The dashed orange line connects the data points to guide the eyes. (b)–(f) Averaged momentum spectra used to obtain the data points marked in (a) by the symbols highlighted in black. We chose the same parameters as for the data presented in figure 1. Since the system spontaneously picks one of the two possible phases of the DTC state, we first extract the time phase as in figure 1(c) from a Fourier spectrum and then post-select realizations with similar phase values before averaging. More details about the post-selection process are found in the supplementary information together with a video showing the time evolution of the momentum spectra. (g) Phases of the oscillations of $N_{\mathrm{P}}(t)$. The error bars show statistical errors for averaging over multiple realizations.

significantly decrease as the response locks onto the subharmonic of the drive. Moreover, frequency locking is reached for smaller f_0 when using a square wave or sinusoidal modulation when compared to a sawtooth modulation. This may be explained as follows: the modulation is implemented as $\varepsilon(t) = \varepsilon_{\mathrm{f}}[1 + f_0\, g(t)]$, where $g(t)$ denotes one of the three waveforms oscillating between the maximal and minimal values 1 and -1. For this specification of f_0, the amplitude of the fundamental harmonic contribution of the square, sinusoidal, and sawtooth waveforms are $\{4/\pi, 1, 2/\pi\}$, respectively. Hence, when compared to the sinusoidal waveform, the square wave and the sawtooth modulation should produce tighter or weaker locking, respectively. For the square wave, however, the higher harmonic components give rise to increased heating, which reduces the atom-cavity coupling and hence acts to compensate for the tighter locking.

So far, we have restricted ourselves to obtaining information about the atom-cavity system by analyzing the light field

leaking out of the cavity, which serves as a non-destructive monitor for the light-matter dynamics. However, we also have direct access to the matter sector via momentum spectra measured after a 25 ms long free expansion of the ensemble. This time-of-flight (TOF) technique is destructive, and we need to prepare a new matter sample every time a momentum spectrum is recorded. In the CTC phase, in each experimental realization, the intra-cavity light field and the corresponding matter grating oscillate with a random time phase as a consequence of CTTS breaking (cf figure 1(b)). Hence, averaging over multiple realizations, in order to improve signal-to-noise, washes out the dynamical signatures of the observed momentum distributions. In the DTC regime, only two time phases, differing by π, emerge. These phases can be discriminated by analyzing Fourier spectra according to figure 1(c), such that post-selection allows for averaging momentum spectra with the same phase value. With this, we directly observe the dynamics of the atomic matter grating. In figure 4(a), the time evolution of $N_{\mathrm{P}}(t)$ is plotted as a solid blue line, and the time evolution of the sum N_{11} of the populations of the four momentum modes $\{p_{\mathrm{y}},p_{\mathrm{z}}\}=\{\pm1,\pm1\}\hbar k$, normalized to the total atom number N_{a}, is shown by orange and gray markers. In order to obtain N_{11}/N_{a}, momentum spectra like those shown in figures 4(b)–(f) are recorded, post-selected to only account for similar time phase values, and averaged. We observe an oscillation in the dynamics of N_{11}/N_{a} at a frequency similar to that of the intra-cavity photon number but notably with a time phase shifted relative to the time phase of $N_{\mathrm{P}}(t)$. This retardation between the dynamics of the light field and the matter distribution is a key feature of our recoil resolved atom-cavity system [41, 42] and is consistent with simulations using an idealized model for the atom-cavity system (cf supplementary information). In figure 4(g), the phase of the oscillation of $N_{\mathrm{P}}(t)$ with respect to the phase of the drive is plotted versus ω_{dr}, which is tuned across the resonance $\omega_{\mathrm{dr}}=2\omega_{\mathrm{CTC}}$. The observed dissipation-induced change of the phase, when ω_{dr} is varied, is a characteristic signature of IL or entrainment. The nearly linear decrease with a negative slope is reproduced by the simulations in the supplementary information [33].

5. Conclusion

In conclusion, we have demonstrated dynamical control of a phase transition between two time crystalline phases. Taking the continuous time crystalline phase of a transversally pumped atom-cavity system as a starting point, we have applied external driving at a frequency of approximately twice the frequency of the continuous time crystal. For sufficiently strong driving, the system locks to the external drive in a subharmonic manner, resulting in a discrete time crystal. This phenomenon establishes subharmonic IL of limit cycles of a nonlinear dissipative oscillator in the context of many-body systems. Therefore, we establish a non-trivial interface between classical non-linear dynamics and time crystals, which suggests a vast range of dynamical phenomena to be understood and established in time crystals and related dynamical many-body states [43, 44].

Data availability statement

All data presented in this article can be provided by the authors A H and H K upon request. All data that support the findings of this study are included within the article (and any supplementary files).

Acknowledgments

We thank J Klinder, C Ni, A Bölian, and C Georges for their support during the early stage of the Project. A H acknowledges useful discussions with C Zimmermann and J Marino. J G C thanks R J L Tuquero for helpful discussions. P K thanks M Sauer for assembling video contents in the supplementary material. A H acknowledges support by the QuantERA II Programme that has received funding from the European Union's Horizon 2020 research and innovation programme under Grant Agreement No. 101017733. P K, J S, L M and A H acknowledge the Deutsche Forschungsgemeinschaft (DFG) for funding through SFB-925 - Project 170620586, and the Cluster of Excellence 'Advanced Imaging of Matter' (EXC 2056) - Project No. 390715994. J G C acknowledges funding from the UP System Balik PhD Program (OVPAA-BPhD-2021-04). J S acknowledges support from the German Academic Scholarship Foundation. H K acknowledges funding by the state of North Rhine-Westphalia through the EIN Quantum NRW program and by the Deutsche Forschungsgemeinschaft (DFG) through Grant DFG-KE 2481/1-1. L M acknowledges co-funding by ERDF of the European Union and by 'Fonds of the Hamburg Ministry of Science, Research, Equalities and Districts (BWFGB)'.

Note: During peer-review of this manuscript, we got to know about related experiments using a coupled electron-nuclear spin system [45].

ORCID iDs

Phatthamon Kongkhambut https://orcid.org/0000-0002-4513-5991
Jayson G Cosme https://orcid.org/0000-0001-9943-4711
Jim Skulte https://orcid.org/0000-0002-9493-5506
Michelle A Moreno Armijos https://orcid.org/0000-0001-8225-0043
Ludwig Mathey https://orcid.org/0000-0003-4341-7335
Andreas Hemmerich https://orcid.org/0000-0002-9941-518X
Hans Keßler https://orcid.org/0000-0002-8501-6145

References

[1] Winfree A T 2001 *The Geometry of Biological Time* vol 12 (Springer)
[2] Wilczek F 2012 Quantum time crystals *Phys. Rev. Lett.* **109** 1
[3] Shapere A D and Wilczek F 2017 Realization of 'time crystal' lagrangians and emergent sisyphus dynamics (arXiv:1708.03348)

[4] Abanin D A, Altman E, Bloch I and Serbyn M 2019 Colloquium: many-body localization, thermalization and entanglement *Rev. Mod. Phys.* **91** 21001
[5] Zaletel M P, Lukin M, Monroe C, Nayak C, Wilczek F and Yao N Y 2023 Colloquium: quantum and classical discrete time crystals *Rev. Mod. Phys.* **95** 031001
[6] Rao R and Esposito M 2016 Nonequilibrium thermodynamics of chemical reaction networks: wisdom from stochastic thermodynamics *Phys. Rev.* X **6** 041064
[7] Iemini F, Russomanno A, Keeling J, Schiró M, Dalmonte M and Fazio R 2018 Boundary time crystals *Phys. Rev. Lett.* **121** 35301
[8] Keßler H, Cosme J G, Hemmerling M, Mathey L and Hemmerich A 2019 Emergent limit cycles and time crystal dynamics in an atom-cavity system *Phys. Rev.* A **99** 1
[9] Buča B, Tindall J and Jaksch D 2019 Non-stationary coherent quantum many-body dynamics through dissipation *Nat. Commun.* **10** 1730
[10] Zhang J *et al* 2017 Observation of a discrete time crystal *Nature* **543** 217
[11] Choi S *et al* 2017 Observation of discrete time-crystalline order in a disordered dipolar many-body system *Nature* **543** 221
[12] Smits J, Liao L, Stoof H T and Straten P V D 2018 Observation of a space-time crystal in a superfluid quantum gas *Phys. Rev. Lett.* **121** 185301
[13] Keßler H, Kongkhambut P, Georges C, Mathey L, Cosme J G and Hemmerich A 2021 Observation of a dissipative time crystal *Phys. Rev. Lett.* **127** 43602
[14] Kongkhambut P, Keßler H, Skulte J, Mathey L, Cosme J G and Hemmerich A 2021 Realization of a periodically driven open three-level dicke model *Phys. Rev. Lett.* **127** 253601
[15] Zhu B, Marino J, Yao N Y, Lukin M D and Demler E A 2019 Dicke time crystals in driven-dissipative quantum many-body systems *New J. Phys.* **21** 073028
[16] Skulte J, Kongkhambut P, Keßler H, Hemmerich A, Mathey L and Cosme J G 2021 Parametrically driven dissipative three-level dicke model *Phys. Rev.* A **104** 063705
[17] Taheri H, Matsko A B, Maleki L and Sacha K 2022 All-optical dissipative discrete time crystals *Nat. Commun.* **13** 848
[18] Autti S, Eltsov V B and Volovik G E 2018 Observation of a time quasicrystal and its transition to a superfluid time crystal *Phys. Rev. Lett.* **120** 215301
[19] Kongkhambut P, Skulte J, Mathey L, Cosme J G, Hemmerich A and Keßler H 2022 Observation of a continuous time crystal *Science* **377** 670
[20] Greilich A, Kopteva N E, Kamenskii A N, Sokolov P S, Korenev V L and Bayer M 2024 Robust continuous time crystal in an electron-nuclear spin system *Nat. Phys.* **20** 631
[21] Liu T, Ou J Y, MacDonald K F and Zheludev N I 2023 Photonic metamaterial analogue of a continuous time crystal *Nat. Phys.* **19** 986
[22] Chen Y H and Zhang X 2023 Realization of an inherent time crystal in a dissipative many-body system *Nat. Commun.* **14** 6161
[23] Strogatz S H 2015 *Nonlinear Dynamics and Chaos* (CRC Press, Taylor & Francis Group)
[24] Jensen M H, Bak P and Bohr T 1983 Complete devil's staircase, fractal dimension and universality of mode-locking structure in the circle map *Phys. Rev. Lett.* **50** 1637
[25] Jensen M H, Bak P and Bohr T 1984 Transition to chaos by interaction of resonances in dissipative systems.i. circle maps *Phys. Rev.* A **30** 1960
[26] Daan S and Aschoff J 2001 *The Entrainment of Circadian Systems* (Springer) pp 7–43
[27] Hanson F E, Case J F, Buck E and Buck J 1971 Synchrony and flash entrainment in a new guinea firefly *Science* **174** 161
[28] Piazza F and Ritsch H 2015 Self-ordered limit cycles, chaos and phase slippage with a superfluid inside an optical resonator *Phys. Rev. Lett.* **115** 163601
[29] Keßler H, Cosme J G, Georges C, Mathey L and Hemmerich A 2020 From a continuous to a discrete time crystal in a dissipative atom-cavity system *New J. Phys.* **22** 085002
[30] Colella E, Kosior A, Mivehvar F and Ritsch H 2022 Open quantum system simulation of faraday's induction law via dynamical instabilities *Phys. Rev. Lett.* **128** 070603
[31] Nie X and Zheng W 2023 Mode softening in time-crystalline transitions of open quantum systems *Phys. Rev.* A **107** 033311
[32] Skulte J, Kongkhambut P, Keßler H, Hemmerich A, Mathey L, and Cosme J G 2024 Realizing limit cycles in dissipative bosonic systems (arXiv:2401.05332)
[33] Supplementary information including more details about the experimental setup, theoretical model, and additional experiments
[34] Giergiel K, Miroszewski A and Sacha K 2018 Time Crystal Platform: from quasicrystal structures in time to systems with exotic interactions *Phys. Rev. Lett.* **120** 140401
[35] Keßler H, Klinder J, Wolke M and Hemmerich A 2014 Optomechanical atom-cavity interaction in the sub-recoil regime *New J. Phys.* **16** 53008
[36] Klinder J, Keßler H, Georges C, Vargas J and Hemmerich A 2016 Bose-einstein condensates in an optical cavity with sub-recoil bandwidth *Appl. Phys.* B **122** 765
[37] Black A T, Chan H W and Vuletic V V 2003 Observation of collective friction forces due to spatial self-organization of atoms: from Rayleigh to Bragg scattering *Phys. Rev. Lett.* **91** 203001
[38] Baumann K, Guerlin C, Brennecke F and Esslinger T 2010 Dicke quantum phase transition with a superfluid gas in an optical cavity *Nature* **464** 1301
[39] Klinder J, Keßler H, Wolke M, Mathey L and Hemmerich A 2015 Dynamical phase transition in the open Dicke model *Proc. Natl Acad. Sci.* **112** 3290
[40] Baumann K, Mottl R, Brennecke F and Esslinger T 2011 Exploring symmetry breaking at the dicke quantum phase transition *Phys. Rev. Lett.* **107** 140402
[41] Keßler H, Klinder J, Venkatesh B P, Georges C and Hemmerich A 2016 In situ observation of optomechanical bloch oscillations in an optical cavity *New J. Phys.* **18** 102001
[42] Georges C, Vargas J, Keßler H, Klinder J and Hemmerich A 2017 Bloch oscillations of a bose-einstein condensate in a cavity-induced optical lattice *Phys. Rev.* A **96** 063615
[43] Liu B *et al* 2024 Higher-order and fractional discrete time crystals in Floquet-driven Rydberg atoms (arXiv:2402.13657)
[44] He G, Ye B, Gong R, Yao C, Liu Z, Murch K W, Yao N Y and Zu C 2024 Experimental realization of discrete time quasi-crystals (arXiv:2403.17842)
[45] Greilich A, Kopteva N E, Korenev V L and Bayer M 2024 Exploring nonlinear dynamics in periodically driven time crystal: from synchronized to chaotic motion (arXiv:2406.06243)